

# Scalable cardiac electro-mechanical solvers and reentry dynamics

P. Colli Franzone, L. F. Pavarino, S. Scacchi, and S. Zampini

**Abstract** We present a scalable solver for the three-dimensional cardiac electro-mechanical coupling (EMC) model, which represents, currently, the most complete mathematical description of the interplay between the electrical and mechanical phenomena occurring during a heartbeat. The most computational demanding parts of the EMC model are: the electrical current flow model of the cardiac tissue, called Bidomain model, consisting of two non-linear partial differential equations of reaction-diffusion type; the quasi-static finite elasticity model for the deformation of the cardiac tissue. Our finite element parallel solver is based on: Block Jacobi and Multilevel Additive Schwarz preconditioners for the solution of the linear systems deriving from the discretization of the Bidomain equations; Newton-Krylov-Algebraic-Multigrid or Newton-Krylov-BDDC algorithms for the solution of the non-linear algebraic system deriving from the discretization of the finite elasticity equations. Three-dimensional numerical test on two linux clusters show the effectiveness and scalability of the EMC solver in simulating both physiological and pathological cardiac dynamics.

---

P. Colli Franzone

University of Pavia, Dept. of Mathematics, Via Ferrata 5, 27100 Pavia, Italy, e-mail: colli@imati.cnr.it

L. F. Pavarino

University of Pavia, Dept. of Mathematics, Via Ferrata 5, 27100 Pavia, Italy, e-mail: luca.pavarino@unipv.it

S. Scacchi

University of Milano, Dept. of Mathematics, Via Saldini 50, 20133 Milano, Italy, e-mail: simone.scacchi@unimi.it

S. Zampini

Extreme Computing Research Center, Computer Electrical and Mathematical Sciences & Engineering Department, King Abdullah University of Science and Technology, Saudi Arabia e-mail: stefano.zampini@kaust.edu.sa

## 1 Introduction

In the last twenty years, computer modeling has become an effective tool to push forward the understanding of the fundamental mechanisms underlying the origin of life-threatening arrhythmias and contractile disorders in the human heart and to provide theoretical support to cardiologists in developing more successful pharmacological and surgical treatments for these pathologies.

The spread of the electrical impulse in the cardiac muscle and the subsequent contraction-relaxation process are quantitatively described by the cardiac electro-mechanical coupling (EMC) model, which consists of the following four components: the quasi-static finite elasticity model of the deforming cardiac tissue, derived from a strain energy function which characterizes the anisotropic mechanical properties of the myocardium; the active tension model, consisting of a system of non-linear ordinary differential equations (ODEs), describing the intracellular calcium dynamics and cross bridges binding; the electrical current flow model of the cardiac tissue, called Bidomain model, which is a degenerate parabolic system of two non-linear partial differential equations of reaction-diffusion type, describing the evolution in space and time of the intra- and extracellular electric potentials; the membrane model of the cardiac myocyte, i.e. a stiff system of ODEs, describing the flow of the ionic currents through the cellular membrane.

This complex non-linear model poses great theoretical and numerical challenges. At the numerical level, the approximation and simulation of the cardiac EMC model is a very demanding and expensive task, because of the very different space and time scales associated with the electrical and mechanical models, as well as their non-linear and multiphysics interactions.

In this paper, we present the finite element solver that we have developed to simulate the cardiac electro-mechanical activity on parallel computational platforms. The solver is based on a Multilevel Additive Schwarz preconditioner for the linear system arising from the discretization of the Bidomain model and on a Newton-Krylov-BDDC method for the non-linear system arising from the discretization of finite elasticity. Three-dimensional numerical tests show the effectiveness and scalability of the solver on Linux clusters, in both normal physiological and pathological situations.

## 2 Cardiac electro-mechanical models

**a) Mechanical model of cardiac tissue.** The deformation of the cardiac tissue is described by the equations of three-dimensional non-linear elasticity

$$\text{Div}(\mathbf{FS}) = \mathbf{0}, \quad \mathbf{X} \in \widehat{\Omega}, \quad (1)$$

where  $\mathbf{X} = (X_1, X_2, X_3)^T$  are the material coordinates of the undeformed cardiac domain  $\widehat{\Omega}$  ( $\mathbf{x} = (x_1, x_2, x_3)^T$  are the spatial coordinates of the deformed cardiac do-

main  $\Omega(t)$  at time  $t$ ), and  $\mathbf{F}(\mathbf{X}, t) = \frac{\partial \mathbf{x}}{\partial \mathbf{X}}$  is the deformation gradient. The second Piola-Kirchhoff stress tensor  $\mathbf{S} = \mathbf{S}^{pas} + \mathbf{S}^{vol} + \mathbf{S}^{act}$  is assumed to be the sum of passive, volumetric and active components. The passive and volumetric components are defined as

$$S_{ij}^{pas,vol} = \frac{1}{2} \left( \frac{\partial W^{pas,vol}}{\partial E_{ij}} + \frac{\partial W^{pas,vol}}{\partial E_{ji}} \right) \quad i, j = 1, 2, 3, \quad (2)$$

where  $\mathbf{E} = \frac{1}{2}(\mathbf{C} - \mathbf{I})$  and  $\mathbf{C} = \mathbf{F}^T \mathbf{F}$  are the Green-Lagrange and Cauchy strain tensors,  $W^{pas}$  is an exponential strain energy function (derived from [7]) modeling the myocardium as an orthotropic (or transversely isotropic) hyperelastic material, and  $W^{vol} = K(J - 1)^2$  is a volume change penalization term accounting for the nearly incompressibility of the myocardium, with  $K$  a positive bulk modulus and  $J = \det(\mathbf{F})$ .

**b) Mechanical model of active tension.** The active component of the stress tensor is given by  $\mathbf{S}^{act} = T_a \frac{\hat{\mathbf{a}}_l \otimes \hat{\mathbf{a}}_l}{\hat{\mathbf{a}}_l^T \mathbf{C} \hat{\mathbf{a}}_l}$ , where  $\hat{\mathbf{a}}_l$  is the fiber direction and  $T_a = T_a \left( C a_i, \lambda, \frac{d\lambda}{dt} \right)$  is the fiber active tension, obtained by solving a biochemical differential system depending on intracellular calcium concentrations, the myofiber stretch  $\lambda = \sqrt{\hat{\mathbf{a}}_l^T \mathbf{C} \hat{\mathbf{a}}_l}$  and stretch-rate  $\frac{d\lambda}{dt}$  (see [11]).

**c) Bioelectrical model of cardiac tissue: the Bidomain model.** The evolution of the cardiac extracellular and transmembrane potentials  $u_e, v$ , gating variable  $\mathbf{w}$ , and ionic concentrations  $\mathbf{c}$ , is given by the Bidomain model. Its parabolic-elliptic formulation on the deformed configuration  $\Omega(t)$  reads:

$$\begin{cases} c_m \frac{\partial v}{\partial t} - \operatorname{div}(D_i \nabla(v + u_e)) + i_{ion}(v, \mathbf{w}, \mathbf{c}, \lambda) = i_{app} \\ -\operatorname{div}(D_i \nabla v) - \operatorname{div}((D_i + D_e) \nabla u_e) = 0. \end{cases} \quad (3)$$

In the Lagrangian framework, after the pull-back on the reference configuration  $\hat{\Omega} \times (0, T)$ , the Bidomain system becomes

$$\begin{cases} c_m J \left( \frac{\partial \hat{v}}{\partial t} - \mathbf{F}^{-T} \operatorname{Grad} \hat{v} \cdot \mathbf{V} \right) - \operatorname{Div}(J \mathbf{F}^{-1} \hat{D}_i \mathbf{F}^{-T} \operatorname{Grad}(\hat{v} + \hat{u}_e)) + J i_{ion}(\hat{v}, \hat{\mathbf{w}}, \hat{\mathbf{c}}, \lambda) = J \hat{i}_{app} \\ -\operatorname{Div}(J \mathbf{F}^{-1} \hat{D}_i \mathbf{F}^{-T} \operatorname{Grad} \hat{v}) - \operatorname{Div}(J \mathbf{F}^{-1} (\hat{D}_i + \hat{D}_e) \mathbf{F}^{-T} \operatorname{Grad} \hat{u}_e) = 0, \end{cases} \quad (4)$$

where  $c_m$  and  $i_{ion}$  are the membrane capacitance and ionic current per unit volume, respectively, and  $\mathbf{V} = \frac{\partial \mathbf{u}}{\partial t}$  is the rate of deformation; see [4] for the detailed derivation. These two partial differential equations (PDEs) are coupled through the reaction term  $i_{ion}$  with the ODE system of the membrane model, given in  $\Omega(t) \times (0, T)$  by

$$\frac{\partial \mathbf{w}}{\partial t} - \mathbf{R}_w(v, \mathbf{w}) = 0, \quad \frac{\partial \mathbf{c}}{\partial t} - \mathbf{R}_c(v, \mathbf{w}, \mathbf{c}) = 0. \quad (5)$$

This system is completed by prescribing initial conditions, insulating boundary conditions, and the applied current  $\hat{i}_{app}$ . Since the extracellular potential  $\hat{u}_e$  is defined up to a time dependent constant in space, we fix it by imposing that  $\hat{u}_e$  has zero aver-

age on the cardiac domain; see [4] for further details. The orthotropic conductivity tensors in the deformed configuration are given by

$$D_{i,e} = \sigma_t^{i,e} I + (\sigma_l^{i,e} - \sigma_t^{i,e}) \mathbf{a}_l \otimes \mathbf{a}_l + (\sigma_n^{i,e} - \sigma_t^{i,e}) \mathbf{a}_n \otimes \mathbf{a}_n,$$

where  $\sigma_l^{i,e}$ ,  $\sigma_t^{i,e}$ ,  $\sigma_n^{i,e}$  are the conductivity coefficients in the intra- and extracellular media measured along and across the fiber direction  $\mathbf{a}_l, \mathbf{a}_t, \mathbf{a}_n$ .

**d) Ionic membrane model and stretch-activated channel current.** The ionic current in the Bidomain model (3) is  $i_{ion} = \chi I_{ion}$ , where  $\chi$  is the membrane surface to volume ratio and  $I_{ion}(v, \mathbf{w}, \mathbf{c}, \lambda) = I_{ion}^m(v, \mathbf{w}, \mathbf{c}) + I_{sac}(v, \mathbf{c}, \lambda)$  is the sum of the ionic term  $I_{ion}^m(v, \mathbf{w}, \mathbf{c})$  given by the ten Tusscher model (TP06) consisting of 17 ordinary differential equations, [20, 21], available from the cellML depository (models.cellml.org/cellml), and a stretch-activated current  $I_{sac}$ . In this work, we adopt the model of  $I_{sac}$  proposed in [13] as the sum of non-selective and selective currents  $I_{sac} = I_{ns} + I_{Ko}$ . We will consider two calibrations where the  $I_{sac}$  equilibrium potential (denoted in the following by  $V_{sac}$ , i.e. the value such that  $I_{sac}(V_{sac}) = 0$ ) is either  $V_{sac} = -60 \text{ mV}$  or  $V_{sac} = -19 \text{ mV}$ . We recall that, for  $v > V_{sac}$ , the stretch-activated current  $I_{sac}$  is positive, thus it has a hyperpolarizing effect, while, for  $v < V_{sac}$ ,  $I_{sac}$  is negative, resulting in a depolarizing effect. For further details, we refer to [5].

### 3 Numerical methods

**Space discretization.** We discretize the cardiac domain with a hexahedral structured grid  $T_{hm}$  for the mechanical model (1) and  $T_{he}$  for the electrical Bidomain model (4), where  $T_{he}$  is a refinement of  $T_{hm}$ . We then discretize all scalar and vector fields of both mechanical and electrical models by isoparametric  $Q_1$  finite elements in space.

**Time discretization.** The time discretization is performed by a semi-implicit splitting method, where the electrical and mechanical time steps can be different. At the  $n$ -th time step,

a) given  $v^n, w^n, c^n$ , solve the ODE system of the membrane model with a first-order IMEX method to compute the new  $w^{n+1}, c^{n+1}$ .

b) given the calcium concentration  $Ca_i^{n+1}$ , which is included in the concentration variables  $c^{n+1}$ , solve the mechanical problems (1) and the active tension differential system to compute the new deformed coordinates  $\mathbf{x}^{n+1}$ , providing the new deformation gradient tensor  $\mathbf{F}_{n+1}$ .

c) given  $w^{n+1}, c^{n+1}, \mathbf{F}_{n+1}$  and  $J_{n+1} = \det(\mathbf{F}_{n+1})$ , solve the Bidomain system (4) with a first order IMEX method and compute the new electric potentials  $v^{n+1}, u_e^{n+1}$  with an operator splitting method, where the parabolic and elliptic PDEs are decoupled; see [4] for further details.

## 4 Parallel solver

### 4.1 Computational kernels

Due to the discretization strategies described above, the main computational kernels of our solver at each time step are the following:

- 1- solve the non-linear system deriving from the discretization of the mechanical problem (1) using an inexact Newton method. At each Newton step, a non-symmetric Jacobian system  $Kx = f$  is solved inexactly by the GMRES iterative method preconditioned by a BDDC preconditioner, described in the next section.
- 2- solve the two linear systems deriving from the discretization of the parabolic and elliptic equations of the Bidomain model, by using the Conjugate Gradient method preconditioned by the Block Jacobi and Multilevel Additive Schwarz preconditioners, respectively, developed in [14].

### 4.2 Mechanical solver

**Schur Complement System.** To keep the notation simple, in the remainder of this section and the next, we denote the reference domain by  $\Omega$  instead of  $\hat{\Omega}$ . Let us consider a decomposition of  $\Omega$  into  $N$  nonoverlapping subdomains  $\Omega_i$  of diameter  $H_i$  (see e.g. [22, Ch. 4])  $\Omega = \bigcup_{i=1}^N \Omega_i$ , and set  $H = \max H_i$ . As in classical iterative substructuring, we reduce the problem to the interface  $\Gamma := \left( \bigcup_{i=1}^N \partial\Omega_i \right) \setminus \partial\Omega$  by eliminating the interior degrees of freedom associated to basis functions with support in the interior of each subdomain, hence obtaining the Schur complement system

$$S_\Gamma x_\Gamma = g_\Gamma, \quad (6)$$

where  $S_\Gamma = K_{\Gamma\Gamma} - K_{\Gamma I} K_I^{-1} K_{I\Gamma}$  and  $g_\Gamma = f_\Gamma - K_{\Gamma I} K_I^{-1} f_I$  are obtained from the original discrete problem  $Kx = f$  by reordering the finite element basis functions in interior (subscript  $I$ ) and interface (subscript  $\Gamma$ ) basis functions.

**BDDC preconditioner.** The Schur complement system (6) is solved iteratively by the GMRES method using a BDDC preconditioner  $M_{BDDC}^{-1}$

$$M_{BDDC}^{-1} S_\Gamma x_\Gamma = M_{BDDC}^{-1} g_\Gamma. \quad (7)$$

Once the interface solution  $x_\Gamma$  is computed, the internal values  $x_I$  can be recovered by solving local problems on each subdomain  $\Omega_i$ .

BDDC preconditioners represent an evolution of balancing Neumann-Neumann methods where all local and coarse problems are treated additively due to a choice of so-called primal continuity constraints across the interface of the subdomains. These primal constraints can be point constraints and/or averages or moments over edges or faces of the subdomains. BDDC preconditioners were introduced in [6] and first

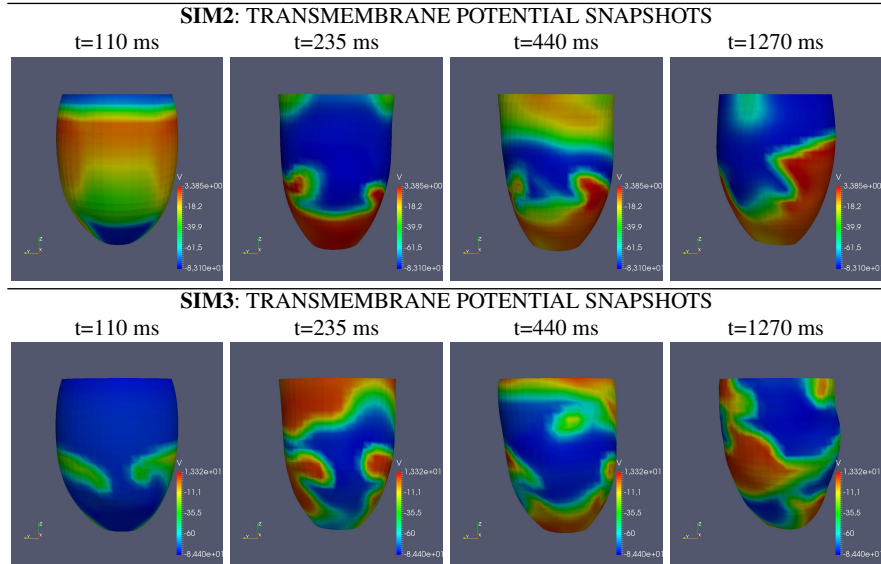


**Fig. 1** Test 1: Snapshots of transmembrane potentials computed from **SIM2** (ventricular tachycardia) and **SIM3** (ventricular fibrillation). The units in the colorbars are given in  $mV$ .

analyzed in [12]. We remark that BDDC is closely related to FETI-DP algorithms, see, e.g. [10, 9], defined with the same set of primal constraints as BDDC, since it is known that in such a case the BDDC and FETI-DP operators have the same eigenvalues with the exception of zeros and ones. For the construction of BDDC preconditioners applied to the non-linear elasticity system constituting the cardiac electromechanical coupling problem, we refer to [16].

## 5 Numerical Results

In this section, we present the results of parallel numerical experiments performed on the Linux cluster Marconi (<http://www.hpc.cineca.it/hardware/marconi>) of the Cineca Consortium ([www.cineca.it](http://www.cineca.it)). Our code is built on top of the FORTRAN90 wrappers of the open source PETSc library [1]. In the mechanical solver, at each Newton iteration, the non-symmetric Jacobian system is solved iteratively by GMRES preconditioned by the BoomerAMG or the BDDC preconditioner, with zero initial guess and stopping criterion a  $10^{-8}$  reduction of the relative residual  $l_2$ -norm. The BDDC method is available as a preconditioner in PETSc and it has been contributed to the library by S. Zampini, see [25].

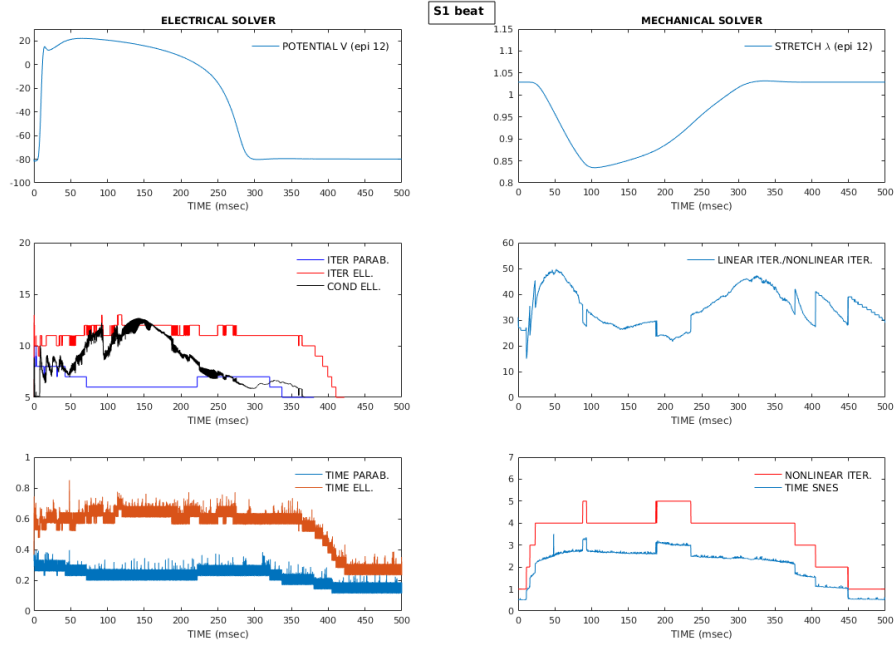


**Fig. 2** S1 beat of physiological test **SIM1** over 500 msec.: time plots at an epicardial point of the indicated electrical (left) and mechanical (right) quantities

### 5.1 Test 1: comparison of solver performance on normal and pathological dynamics

We consider an idealized left ventricle, represented by a truncated ellipsoid discretized by an electrical grid of  $384 \times 192 \times 48 Q^1$  finite elements, yielding a total amount of about  $3.6 \cdot 10^6$  nodes, thus the degrees of freedom (dofs) of the parabolic and elliptic Bidomain linear systems are  $3.6 \cdot 10^6$ . The mechanical mesh is eight times coarser than the electrical one, i.e.  $48 \times 24 \times 6 Q^1$  finite elements, with a total amount of 8400 nodes, thus the dofs of the finite elasticity non-linear system are 25200. The electrical time step is 0.05 ms, while the mechanical time step is 0.5 ms. The simulations are run on 24 processors. The tissue is assumed to be axisymmetric. The mechanical non-linear system is solved by the Newton-Krylov-AMG method.

We first compare the performance of the electro-mechanical solver in three different situations:

- a normal physiological heartbeat (**SIM1**) without reentry;
- a ventricular tachycardia dynamics (**SIM2**), with  $V_{sac} = -19$  mV;
- a ventricular fibrillation dynamics (**SIM3**), with  $V_{sac} = -60$  mV.

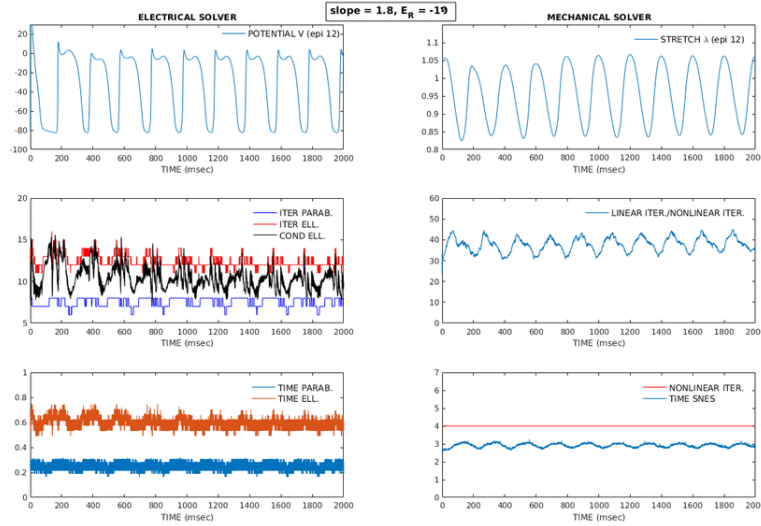


**Fig. 3** Periodic test **SIM2** with slope = 1.8,  $V_{sac} = -19$  mV over 2000 msec.: time plots at an epicardial point of the indicated electrical (left) and mechanical (right) quantities

In **SIM1**, the external stimulus is applied at the endocardial apical region, the interior bottom part of the truncated ellipsoid, and the total simulation run is 500 ms. The activation wavefront propagates starting from the endocardial apical regions, where the stimulus is delivered, towards the whole ventricle (not shown, but similar to the propagation displayed in Fig. 6).

In **SIM2** and **SIM3**, we apply first an S1 stimulus as in **SIM1**. 280 ms after the S1 stimulus is delivered, we apply a premature S2 cross-gradient stimulation current from the base to the apex and across the wall thickness, covering about a third of ventricular volume, to induce a ventricular reentry consisting of a pair of counter-rotating scroll waves. We run the simulation for 2000 ms after the S2 delivery. The SAC parameter  $V_{sac}$  is set to  $-19$  mV and  $-60$  mV in **SIM2** and **SIM3**, respectively.

In **SIM2**, the two scroll waves generated by the S2 stimulus continue to rotate without breaking, leading to a stable periodic ventricular tachycardia pattern, see Fig. 1.

In **SIM3** instead, after the first rotation, the two scroll waves break up into several smaller scroll waves, generating irregular transmembrane potential distributions characterized by high electrical turbulence, often associated with ventricular fibrillation, as shown in the snapshots of Fig. 1. Thus, the low SAC reversal potential ( $V_{sac} = -60$  mV) seems to induce deterioration of the stability of scroll waves, promoting the onset of ventricular fibrillation.

Figures 2, 3, 4 report the time evolution of the mathematical parameters of the electro-mechanical solver (CG iterations, condition numbers, Newton iterations, GMRES iterations) and the CPU times needed to solve the parabolic, elliptic and

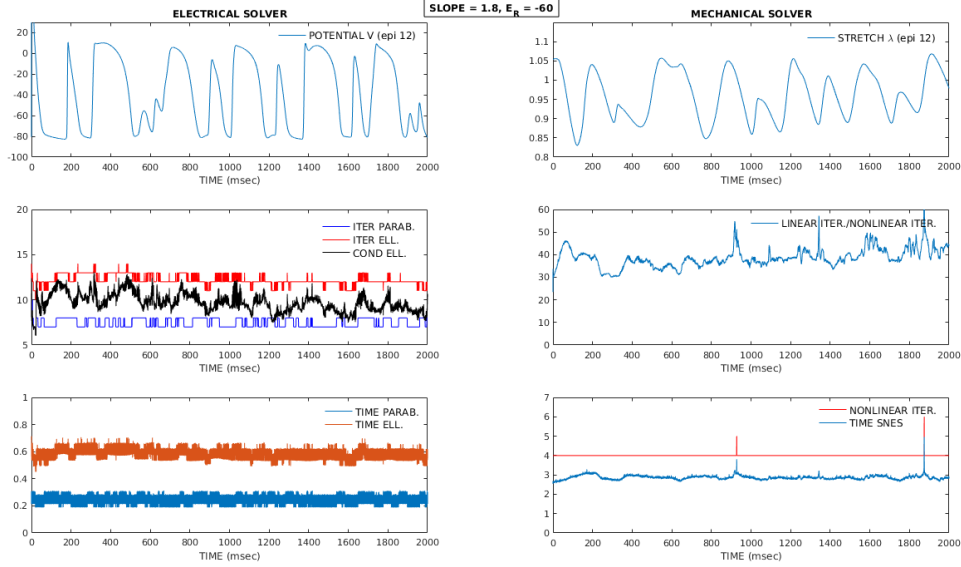


**Fig. 4** Turbulent test **SIM3** with slope = 1.8,  $V_{sac} = -60$  mV over 2000 msec.: time plots at an epicardial point of the indicated electrical (left) and mechanical (right) quantities

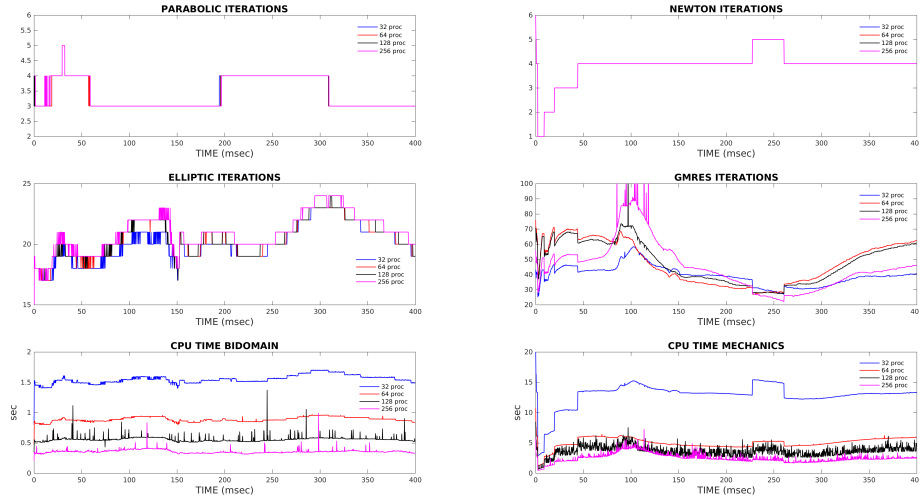
proc	$\Pi = V$		$\Pi = VE$	
	$\bar{it}_{par}$	$time_{par}$	$\bar{it}_{ell}$	$time_{ell}$
32	3	2.24e-1	20	9.56e-1
64	3	1.24e-1	20	5.37e-1
128	3	7.71e-2	20	3.17e-1
256	3	3.78e-2	20	2.40e-1

proc	$\Pi = V$		$\Pi = VE$	
	$\bar{nit}$	$\bar{lit}$	$\bar{nit}$	$\bar{lit}$
32	4	39	4	38
64	4	48	4	47
128	4	48	4	47
256	4	45	4	44

**Table 1** Strong scaling test on a whole heartbeat simulation.  $\bar{it}_{par}$ : CG iteration to solve the parabolic linear system (average per time step).  $time_{par}$ : CPU time to solve the parabolic linear system (average per time step).  $\bar{it}_{ell}$ : CG iteration to solve the elliptic linear system (average per time step).  $time_{ell}$ : CPU time to solve the elliptic linear system (average per time step).  $\bar{nit}$ : Newton iteration to solve the mechanical system (average per time step).  $\bar{lit}$ : GMRES iteration to solve the Jacobian system (average per Newton iteration).  $time_{snes}$ : CPU time to solve the mechanical system (average per time step). All CPU times are given in seconds.

non-linear systems (TIME PARAB., TIME ELL., TIME SNES, respectively) obtained from the **SIM1**, **SIM2**, **SIM3**, respectively. The results show that all the components of the solver are quite robust with respect to the different simulation dynamics considered, physiological and pathological. The condition number of the elliptic solver increases slightly when the contraction is more pronounced, but it always remains bounded between 10 and 15.



**Fig. 5** Strong scaling test on a whole heartbeat simulation. Time evolution of electrical and mechanical solvers parameters.

## 5.2 Test 2: strong scaling on a normal heartbeat

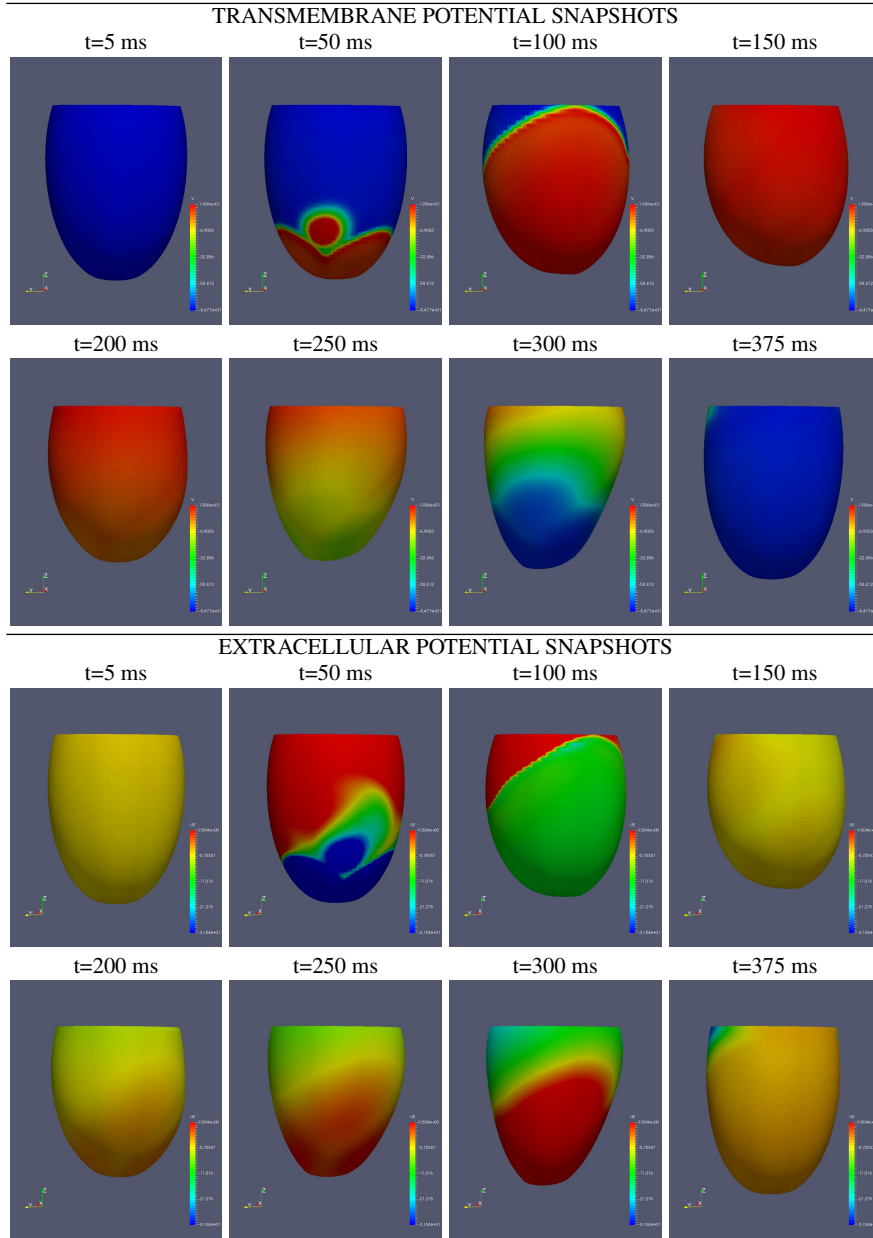
We then perform a strong scaling test on a whole heartbeat lasting 400 *ms*. The three-dimensional cardiac domain considered is a truncated ellipsoid modeling the left ventricle, discretized by an electrical mesh of  $384 \cdot 192 \cdot 48 Q_1$  finite elements, yielding the same Bidomain dofs as in the previous test, about  $3.6 \cdot 10^6$ . The mechanical mesh size is now four times coarser than the electrical one in each direction, thus the mechanical elements are  $96 \cdot 48 \cdot 12$ , resulting in 183456 displacement dofs. The number of subdomains (processors) increases from 32 to 256 whereas the number of degrees of freedom per subdomain is reduced as the number of subdomains increases. The tissue is assumed to be orthotropic. The mechanical non-linear system is solved by the Newton-Krylov-BDDC method. We choose as BDDC primal constraints vertices ( $\Pi = V$ ) and vertices + edges ( $\Pi = VE$ ). To start the electrical excitation, the external stimulus is applied at the endocardial apical region, in four points modeling an idealized Purkinje network.

Fig. 6 reports selected snapshots of transmembrane and extracellular potentials on the deforming domain during the entire heartbeat. The results reported in Table 1 (averages) and Fig. 5 (time evolution) show a good scalability of both the electrical and mechanical components of the parallel solver, with linear and non-linear iterations remaining about constant, while the CPU times decrease when the number of processors increases.

## References

1. S. Balay et al. PETSc users manual. Tech. Rep. ANL-95/11 - Revision 3.3, Argonne National Laboratory, 2012.
2. D. Chapelle et al. An energy-preserving muscle tissue model: formulation and compatible discretizations. *J. Multiscale Comput. Engrg.*, 10:189–211, 2012.
3. P. Colli Franzone, L. F. Pavarino, and S. Scacchi. *Mathematical Cardiac Electrophysiology*. Springer, MSA Vol. 13, New York, 2014.
4. P. Colli Franzone, L. F. Pavarino, and S. Scacchi. Bioelectrical effects of mechanical feedbacks in a strongly coupled cardiac electro-mechanical model. *Math. Mod. Meth. Appl. Sci.*, 26:27–57, 2016.
5. P. Colli Franzone, L. F. Pavarino, and S. Scacchi. Effects of mechanical feedback on the stability of cardiac scroll waves: A bidomain electro-mechanical simulation study. *Chaos*, 27:093905, 2017.
6. C. R. Dohrmann. A preconditioner for substructuring based on constrained energy minimization. *SIAM J. Sci. Comput.*, 25:246–258, 2003.
7. T. S. E. Eriksson et al. Influence of myocardial fiber/sheet orientations on left ventricular mechanical contraction. *Math. Mech. Solids*, 18:592–606, 2013.
8. V. Gurev et al. Models of cardiac electromechanics based on individual hearts imaging data: Image-based electromechanical models of the heart. *Biomech. Model Mechanobiol.*, 10:295–306, 2011.
9. A. Klawonn and O. Rheinbach. Highly scalable parallel domain decomposition methods with an application to biomechanics. *ZAMM-Z. Angew. Math. Mech.*, 90:5–32, 2010.
10. A. Klawonn and O. B. Widlund. Dual-primal FETI methods for linear elasticity. *Comm. Pure Appl. Math.*, 59:1523–1572, 2006.
11. S. Land et al. An analysis of deformation-dependent electromechanical coupling in the mouse heart. *J. Physiol.*, 590:4553–4569, 2012.
12. J. Mandel and C. R. Dohrmann. Convergence of a balancing domain decomposition by constraints and energy minimization. *Numer. Lin. Alg. Appl.*, 10:639–659, 2003.
13. S. A. Niederer and N. P. Smith. A mathematical model of the slow force response to stretch in rat ventricular myocytes. *Biophys. J.*, 92: 4030–4044, 2007.
14. L. F. Pavarino and S. Scacchi. Multilevel additive Schwarz preconditioners for the Bidomain reaction-diffusion system. *SIAM J. Sci. Comput.*, 31:420–443, 2008.
15. L. F. Pavarino, S. Zampini, and O.B. Widlund. BDDC preconditioners for spectral element discretizations of almost incompressible elasticity in three dimensions. *SIAM J. Sci. Comput.*, 32 (6):3604–3626, 2010.
16. L. F. Pavarino, S. Scacchi, and S. Zampini. Newton-krylov-BDDC solvers for non-linear cardiac mechanics. *Comput. Meth. Appl. Mech. Engrg.*, 295:562–580, 2015.
17. G. Plank et al. Algebraic Multigrid Preconditioner for the cardiac bidomain model. *IEEE Trans. Biomed. Engrg.*, 54:585–596, 2007.
18. S. Rossi et al. Orthotropic active strain models for the numerical simulation of cardiac biomechanics. *Int. J. Num. Meth. Biomed. Engrg.*, 28:761–788, 2012.
19. J. Sundnes et al. Improved discretisation and linearisation of active tension in strongly coupled cardiac electro-mechanics simulations. *Comput. Meth. Biomech. Biomed. Engrg.*, 17:604–615, 2014.
20. K. H. W. J. ten Tusscher et al. A model for human ventricular tissue. *Am. J. Phys. Heart. Circ. Physiol.*, 286:H1573–H1589, 2004.
21. K. H. W. J. ten Tusscher and A. V. Panfilov. Alternans and spiral breakup in a human ventricular tissue model. *Am. J. Phys. Heart Circ. Physiol.*, 291: H1088–H1100, 2006.
22. A. Toselli and O. B. Widlund. *Domain Decomposition Methods: Algorithms and Theory*. Springer-Verlag, Berlin, 2004.
23. F. J. Vetter and A. D. McCulloch. Three-dimensional stress and strain in passive rabbit left ventricle: a model study. *Ann. Biomed. Engrg.*, 28:781–792, 2000.

24. S. Zampini. Dual-primal methods for the cardiac bidomain model. *Math. Mod. Meth. Appl. Sci.*, 24:667–696, 2014.
25. S. Zampini. PCBDDC: a class of robust dual-primal preconditioners in PETSc. *SIAM J. Sci. Comput.*, 38(5):S282–S306, 2016.



**Fig. 6** Snapshots of transmembrane and extracellular potentials during a whole heartbeat. The units in the colorbars are given in  $mV$ .